Available online at www.sciencedirect.com
ScienceDirect
Nuclear Instruments and Methods in Physics Research A 565 (2006) 551–560
NUCLEAR INSTRUMENTS & METHODS IN PHYSICS RESEARCH Section A
www.elsevier.com/locate/nima

Performance studies with an ALICE TPC prototype

D. Antończyk[a], J. Baechler[b], R. Bramm[a], R. Campagnolo[b], P. Christiansen[b,*], U. Frankenfeld[a], C. Gonzalez Gutierrez[b], M. Ivanov[c], M. Kowalski[d], L. Musa[b], A. Przybyla[a], for the ALICE TPC Collaboration

[a]*Gesellschaft für Schwerionenforschung mbH, Darmstadt, Germany*
[b]*CERN, CH-1211 Geneva, Switzerland*
[c]*Ruprecht-Karls-Universität, Heidelberg, Germany*
[d]*Institute of Nuclear Physics, Cracow, Poland*

Received 16 May 2006; accepted 8 June 2006
Available online 7 July 2006

Abstract

The main components of the ALICE TPC were tested with cosmic rays and beam particles. An Inner Readout Chamber was fully equipped with front end electronics including the DAQ chain, and operated in combination with a prototype field cage. The noise performance, baseline restoration, and characteristics of the ion tail for different gas mixtures were studied in detail. Furthermore, the spatial resolution for tracks and the particle identification performance over a momentum range from 1–7 GeV/c were measured. The measured specific energy loss was compared with predictions from a photo absorption ionization model.

PACS: 29.40.Cs; 29.40.Gx

Keywords: ALICE; TPC; ALTRO; Neon-based gas mixtures; Space point resolution; Ionization energy loss; Straggling

1. Introduction

The ALICE Time Projection Chamber (TPC) is the main tracking detector in the central section of the ALICE heavy ion experiment at LHC [1]. It is composed of a cylindrical gas volume (barrel), divided into two half volumes of equal size, separated by a 30 μm thick HV electrode to generate the drift field. The field cage has an inner radius of about 80 cm, and an outer radius of about 280 cm, with an overall length of 500 cm in the beam direction. At both ends of the barrel, conventional multi-wire proportional chambers (MWPC) with pad readout are mounted into end plates with 18 trapezoidal sectors each. The Front End electronic Cards (FEC) with an optical interface to the DAQ are connected to the pads of the backplane of the readout chambers via ~8 cm long flat Kapton cables.

The conventional design is optimized for tracking of up to 20,000 charged particles in the acceptance of the TPC ($|\eta| \leqslant 0.9$). The high occupancy environment resulted in a design with a low material budget for the field cage components, a highly segmented pad readout with 570,000 pads, and an innovative FE electronics equipped with on-board digital filters to allow baseline restoration and zero-suppression.

A comprehensive test facility was set up at CERN to test individual components, either separately or jointly with other parts of the detector system.

This paper describes the integral tests performed with the TPC test facility using all final components of the ALICE TPC readout chamber, with the focus on the signal shapes induced on single pads, the efficiency of the ion tail cancellation filters, the space point resolution, and the PID performance.

*Corresponding author. Present address: RISØ, National Laboratory, Frederiks borgvej 399, P.O. 49, 4000 Roskilde, Denmark.
E-mail addresses: Peter.Christiansen@cern.ch, peter.christiansen@risoe.dk (P. Christiansen).

0168-9002/$ - see front matter © 2006 Elsevier B.V. All rights reserved.
doi:10.1016/j.nima.2006.06.022

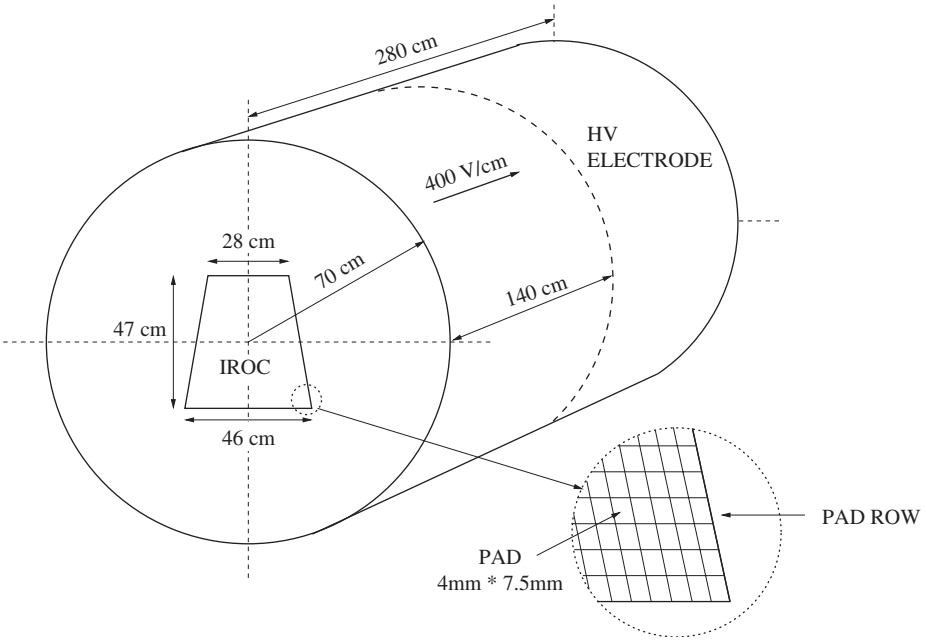

Fig. 1. Schematic of the instrumented TPC prototype field cage.

2. Experimental setup

Fig. 1 gives a schematic view of the TPC prototype. The field cage is a prototype while the readout system consists of an ALICE Inner Readout Chamber (IROC) with the final electronics components. The prototype field cage is also divided into two halves by the central HV electrode, kept at a potential of 55.85 kV, resulting in a drift field of 400 V/cm.

While the tests with cosmic rays were done with the baseline gas mixture of Ne–CO_2 (90–10), the beam test was done using a newly proposed mixture [2] for the final TPC i.e. Ne–CO_2–N_2 (85.7–9.5–4.8). The two gas mixtures have similar drift velocity and diffusion characteristics, but the Ne–CO_2–N_2 mixture provides higher gain stability due to the larger admixture of quencher. The prototype was filled with premixed gas circulating through a cartridge filter of activated copper to keep the oxygen content below 10 ppm.

The gas diffusion constants at 400 V/cm are $D_T = D_L = 220\,\mu m/\sqrt{cm}$, while the drift velocity is about 2.83 cm/μs resulting in an approximate readout time of 50 μs.

One end plate of the prototype field cage was instrumented with an IROC from the ALICE TPC pre-production. The IROC is trapezoidally shaped (see Fig. 1) and its pad plane is segmented into 5504 pads of 4 mm × 7.5 mm arranged in 63 pad rows. The geometry of the three wire grids (gate, cathode, and anode) is described in Ref. [1]. The voltage on the anode wires was 1250 V (Ne–CO_2) and 1480 V (Ne–CO_2–N_2) to achieve an absolute amplification gain of about 20,000 [2]. Despite the significantly higher anode voltage, the stability against glow discharge with Ne–CO_2–N_2 is higher than with Ne–CO_2 [2].

Each pad is read out by a charge sensitive Preamp/Shaper (PASA), a 10-bit 10 MHz low power Analog Digital Converter (ADC),[1] and an Application-Specific Integrated Circuit (ASIC) that contains a digital filter for tail cancellation and baseline restoration as well as zero-suppression circuits and a multi-event buffer. The charge induced on a pad is amplified and integrated via a low input impedance amplifier. The continuously sensitive charge amplifier is followed by a semi-Gaussian pulse shaper of second order. The output of the amplifier/shaper chip is fed into the ALICE TPC Read Out (ALTRO) chip containing 16 channels. Each single FEC reads out 128 electronic channels (pads).

The 43 FECs of the IROC are controlled by two Readout Control Units (RCUs) that transfer the digitized data via the DAQ Detector Data Link (DDL) systems [3] to PCs. The data acquisition was controlled by the standard ALICE DAQ software, DATE version 4.8 [4].

The orientation of the setup was chosen to have the pad rows (anode wires) vertically in the beam test (perpendicular to the beam) and horizontally in the cosmic ray test. This minimizes the influence of angular effects on the spatial resolution.

The trigger signal for the readout electronics was generated from the coincidence of two scintillator counter signals. In the cosmic ray tests the scintillators were positioned above and below the field cage, while in the beam test the scintillators were positioned upstream and downstream of the TPC in the beam line.

[1] In this paper we write ADC for the electronic circuit and ADC channels (ADC ch) for the digital charge measured by the ADC.

Table 1 shows a comparison of prototype parameters with those of the final TPC.

3. Electronics performance

The FECs were designed to have low noise, large dynamic range, and the ability to correct and zero-suppress the digitized signals online [1]. In this section the measured performance is reported. Details of the performance studies can also be found in Refs. [6,7].

Fig. 2 shows the digitized signal from a single pad after the PASA and the ADC. The PASA has a gain of 12 mV/fC, and the ADC in the ALTRO has been selected to have a final conversion factor of 6 ADC ch./fC, with a dynamic range of 10 bits. A Minimum Ionizing Particle (MIP) ionizes about 20 electrons over a distance of 7.5 mm, so with the nominal gas gain, 2×10^4, the most probable value of the maximum charge for a MIP is about 3×10^4 electrons $\approx$30 ADC channels (ADC ch), resulting in a dynamic range of 30 MIPs, which is important for slower particles ($\beta \ll 1$). These conditions were achieved both in the cosmic ray runs and in the beam test.

Using pedestal data the noise fluctuations of the baseline could be measured. For the pads used in the analysis of the track data the noise was found to be $\sigma_{\mathrm{NOISE}} = 0.70 \pm 0.08$ ADC ch $\approx 700 \pm 80$ electrons. This is significantly smaller than the noise requirement of $\sigma_{\mathrm{NOISE}} \leqslant 1000$ electrons [1].

Table 1
Comparison of the ALICE TPC and the prototype

	ALICE TPC	Prototype
Gas volume	88 m^3	4.5 m^3
Maximum drift length	250 cm	140 cm
Drift field	400 V/cm	400 V/cm
Sensitive area	33 m^2	0.17 m^2
Number of pads	557, 568	5504
Number of front end cards	4356	43
Sampling frequency	5.7–11.4 MHz	10 MHz

A table with all relevant parameters for the final TPC can be found in Ref. [5].

The application of a zero-suppression threshold of 3 ADC is foreseen for nominal running of the full TPC. In the worst case of central heavy-ion collisions, this threshold reduces the total data volume for a single event to $\leqslant$60 MB [5]. The requirement of online data reduction without signal loss led to the development of the ALTRO chip. This chip incorporates three functions: ADC, correction filters, and zero suppression. In the remainder of this section we focus on the pad signal ion tail and the corresponding correction filters.

The long tail of the pad signal is caused by the ions as they slowly drift away from the anode wire, and it is a sum of contributions from ions going to the pads, the cathode wires, the gating wires, and escaping into the drift volume, see Ref. [6]. The exact time structure of this tail depends on the field configuration around the anode wire and on the gas mixture. The variation of the ion tail affects the subsequent charge measurements, and, in the high occupancy environment of heavy ion collisions, the cumulative effect of many large signals can shift the baseline by up to 30 ADC ch. The main feature of the ALTRO chip design is its ability to correct for these ion tails and restore the baseline. The action of the digital filter is done in three steps: baseline correction and subtraction 1 (BCS1), ion tail cancellation filter (TCF), and baseline correction and subtraction 2 (BSC2). If necessary the parameters used in each step will be optimized for each pad.

In the first step, BCS1, a time dependent pedestal is subtracted. In the second step, TCF, slowly varying exponential components of the tail are canceled. In the final step, slow non-systematic variations of the baseline are corrected by using a so-called moving average filter.

Fig. 3 shows the passage of a cosmic ray shower through the TPC. Single track events were used to determine the shape of the ion tail, while it was possible to select cosmic ray shower events to test the full ALTRO action on single pad data with occupancies similar to what is expected for central Pb + Pb collisions at LHC.

Fig. 4 shows the average ion tails in the two gas mixtures. The main characteristic of the tails was also reproduced in simulation studies [6]. The signals in the two gases differ in the tail, which can be attributed to the difference in anode voltages.

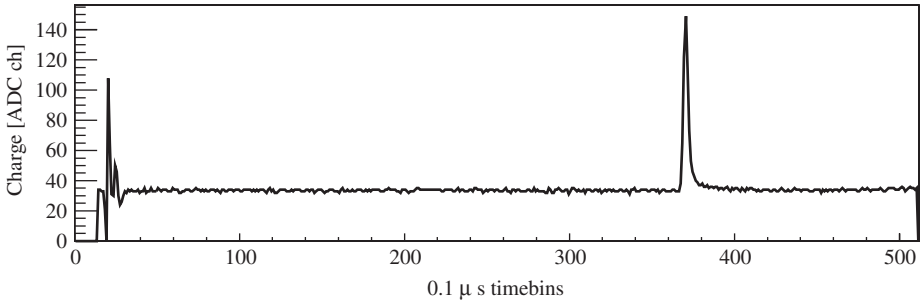

Fig. 2. The signal in a single pad without baseline subtraction. The switching of the gating grid voltages induces the early signal while the signal around time-bin 370 is due to a charged particle.

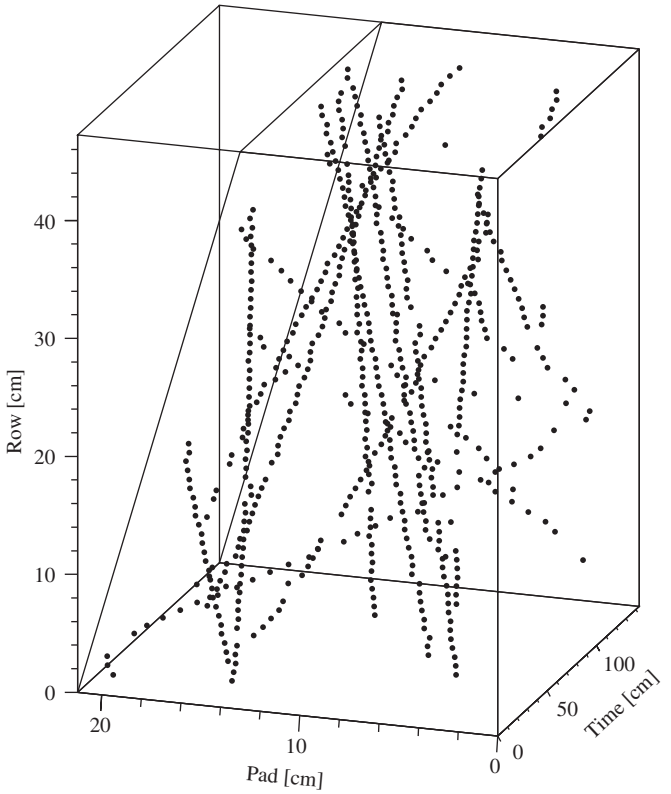

Fig. 3. Tracks from a cosmic ray shower in the TPC reconstructed from the observed ionization. One half of the TPC IROC is shown, and the active volume is illustrated by the trapezoid. The perspective is similar to the one used in Fig. 1.

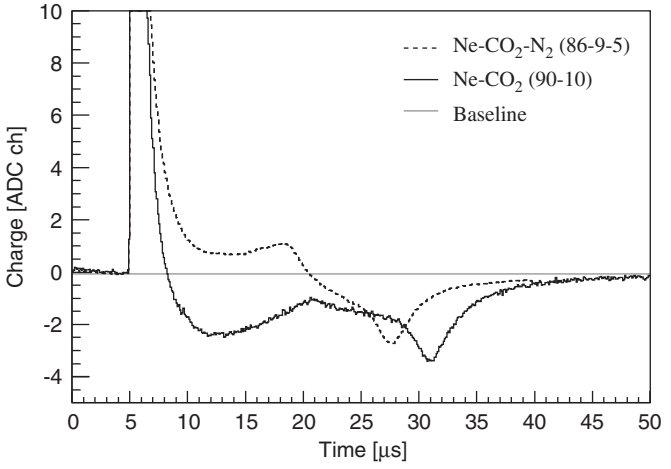

Fig. 4. The shape of the ion tails averaged for large signals. The TCF filter is capable of canceling the slow exponentially decreasing part of the signal observed to around $t = 12\,\mu s$, while the BCS2 filter corrects for the later perturbations of the baseline.

The measurements of the ion tail allowed then the TCF filter to be optimized for the two gases.

The data were recorded without the ALTRO correction filters (BCS1, TCF, BCS2). Instead, the data were used to optimize the filter parameters using corresponding software algorithms [7]. This method is also foreseen for the operation of the ALICE TPC.

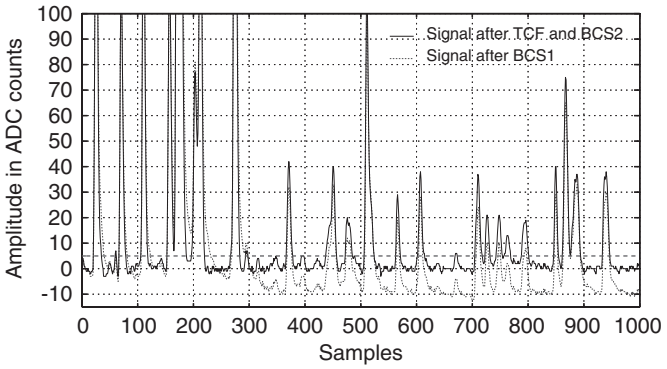

Fig. 5. ALTRO performance on a high occupancy pad.

Fig. 5 shows the signal on a single pad for a cosmic ray shower event before and after the software version of the ALTRO algorithm with optimized parameters was applied. The baseline and low amplitude signals are adequately recovered.

4. Overall detector performance

In the following two sections we discuss space point resolution and particle identification as achieved with our setup.

The word cluster is used to designate the charge signals in a pad row associated with a track. From the cluster information the space point position in the pad and time directions are calculated by simple weighted averages. The total charge Q is the sum of the recorded charge.

4.1. Space point resolution

One of the main goals in the TPC tests was the determination of the space point resolution. This is important for the comparison of the TPC design parameters with those achievable in the real detector, but also in order to verify the Monte Carlo algorithms implemented in the simulation code.

The analysis was performed using the data from the cosmic ray runs with the detector. Tail cancellation and baseline corrections were applied as described in the last section. A simple cluster finding and track finding algorithm was used to reconstruct the space points and tracks. From the total sample of about 7000 events a sub sample of events each containing at most four tracks was chosen to avoid overlapping tracks. To minimize the effect of track inclination we required that the track angle with the time-pad row plane and the pad plane be smaller than 10°. The space point resolution is then determined from the residuals of a straight line fit to the track coordinates in both pad and drift direction as a function of the drift length. Because of the limited number of events the drift volume was divided into six sections with 22.4 cm drift length each.

In Figs. 6 and 7 the results of the analysis are shown, fitted with the following relation:

$$\sigma_{r\phi,z} = \sqrt{\sigma_0^2 + L_{\text{drift}} \cdot \sigma_1^2} \quad (1)$$

where σ_0 is the so-called intrinsic resolution (based on S/N and pad size only) and σ_1 describes the dependence on drift length L_{drift}.

In the drift direction only four points were shown, owing to the fact that for short drift lengths space point coordinates are mainly composed of two-time-bin clusters that significantly deteriorates the resolution in z. Such clusters, however, will not appear in the ALICE TPC because from the collider experiment geometry primary tracks close to the readout chambers have relative large angles with respect to the pad plane effectively widening the clusters in the drift direction.

The data are well represented by the fit, Eq. (1), and the space point resolution at maximal drift length in the ALICE TPC can be derived from the extrapolation of the fit to 250 cm drift length. The comparison (Table 2) of the Monte Carlo studies with the data confirms the viability of the algorithm used in the simulations.

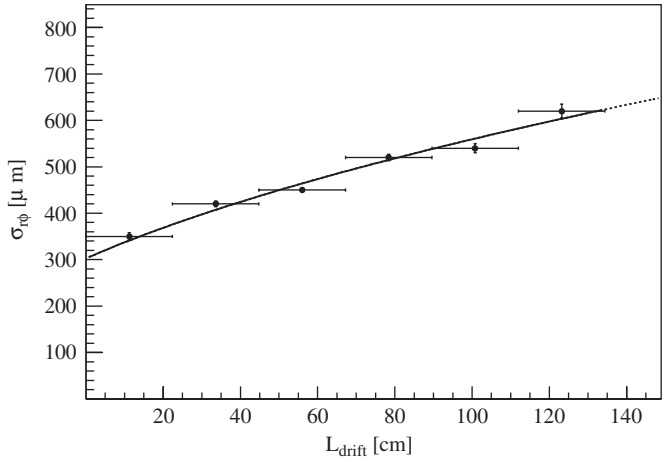

Fig. 6. Space point resolution in pad direction (momentum plane) as a function of drift length. Solid line shows the fit and dashed line the extrapolation.

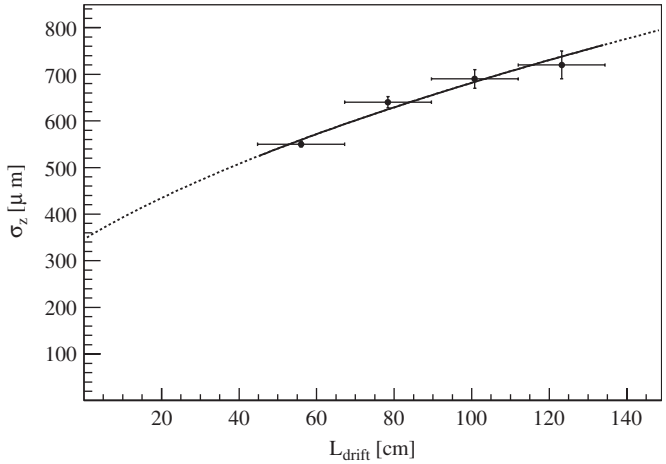

Fig. 7. Space point resolution in drift direction as a function of drift length. Solid line shows the fit and dashed line the extrapolation.

Table 2
Comparison of the space point resolution for 250 cm drift length

	Experiment	Monte Carlo
$\sigma_{r\phi}$ (μm)	800 ± 80	900
σ_z (μm)	900 ± 100	900

4.2. Particle identification

Each reconstructed hit in a track provides a measurement of the deposited charge in addition to the spatial information. The charge collected on the pad is related to the energy loss of the charged particle and it is possible to use this information for particle identification (PID). Here, the PID performance was studied in two different ways using data obtained from the beam test.

(i) *Truncated mean C*: For each track the "truncated mean" C is derived from the average of the 60% lowest cluster charge values. For identical tracks the estimator C is approximately Gaussian distributed, and the relative width of this Gaussian, $\sigma_C \equiv \sigma/\langle C\rangle$, is called the energy loss resolution.

(ii) *The straggling function*: For a given track segment (e.g. the track length over a pad) the cluster-charge-probability-density distribution is denoted the cluster charge straggling function (Landau distribution). The straggling function is a consequence of the underlying energy loss mechanism, and it can be used to fit the cluster charge distribution of a single track taking into account all the cluster information.

First the measurement of the *mean* truncated energy loss $\langle C\rangle$ dependence on $\beta\gamma$, and the resolution will be presented. The results are then compared with model calculations of the ionization energy loss to get a better understanding of the PID performance, but also to investigate the possibilities to exploit PID in the regime of the relativistic rise. The latter requires both an energy loss resolution of better than 7% [5] plus a good understanding of the truncated energy loss distribution, since the separation between π, K and p in that region of $\beta\gamma$ is typically small (of the order 1–4 σ_C).

Data were measured for seven integer (+) momentum settings with $1 \leqslant p \leqslant 7\,\text{GeV}/c$. Only single-track events were analyzed with the first three pad rows ignored because of edge effects in the test setup. After gain corrections, the variation of the average cluster charge over the chamber was less than 3% (RMS). The data were, however, not corrected for pressure and temperature variations.

In all analyzed events the track was located 90 cm from the pad-plane, and was perpendicular to the pad rows and parallel to the pad plane.

The trigger counters were also used to measure the Time-Of-Flight (TOF) of the particles. This allowed us to separate events with a single proton or pion (by more than 6 σ_{TOF}) for momenta up to $p = 3\,\mathrm{GeV}/c$. The high-energy muon background ($p \geqslant 10\,\mathrm{GeV}/c$) present in the low momentum settings unfortunately prevented us from isolating pions.

Furthermore, while it was not possible to isolate pions from protons for $p \geqslant 4\,\mathrm{GeV}/c$, and in general from the background muons, we could nonetheless determine the mean truncated energy loss $\langle C\rangle$ with dual Gaussian fits. Fig. 8 shows the dependence of the mean truncated energy loss $\langle C\rangle$ on $\beta\gamma$. There is a 5% discrepancy in the data between the value of $\langle C\rangle$ measured with $1\,\mathrm{GeV}/c$ pions and with $7\,\mathrm{GeV}/c$ protons. Here the data came from two runs furthest apart in time, and the observed deviation is probably due to pressure and temperature variations between the two runs. Also shown in Fig. 8 are measurements by ALEPH for P10 [1,8] and by NA49 for Ne–CO_2 (90–10) [9]. The dependence of $\langle C\rangle$ on $\beta\gamma$ in the ALICE TPC simulation is based on the ALEPH measurements and the good agreement between all three measurements confirms this assumption.

In the following we use separated protons with $p = 1\,\mathrm{GeV}/c$ (294 tracks), $p = 2\,\mathrm{GeV}/c$ (454 tracks), and $p = 3\,\mathrm{GeV}/c$ (614 tracks). For the straggling function the segment length is given by the pad length of 7.5 mm. The straggling functions and the truncated energy loss distributions are shown in Fig. 9. For the straggling functions the most probable value Δ_p is determined by a Gaussian fit to the peak, and the FWHM w by a fifth-order polynomial fit restricted to the region around the peak. The relative width, w/Δ_p, decreases with increasing Δ_p reflecting the Poisson statistic of the underlying collision cross-section. This leads to an energy loss resolution of $p = 1\,\mathrm{GeV}/c$ protons being better than that of 2 and $3\,\mathrm{GeV}/c$ protons. The probability of a true Gaussian fit to the three truncated mean distributions corresponding to $p = 1, 2, 3\,\mathrm{GeV}/c$ was found to be only 15%, 1.6%, and 0.04%, respectively, indicating that the truncated mean is not strictly Gaussian distributed, with a shoulder at higher C clearly visible.

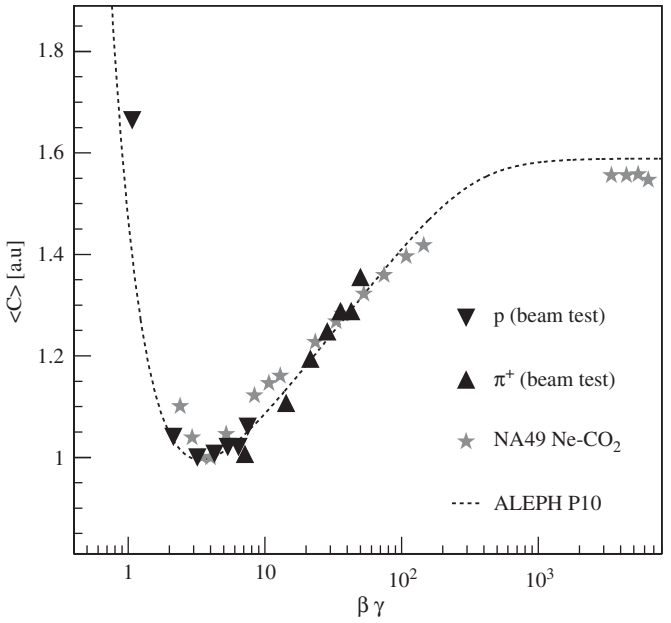

Fig. 8. The average truncated energy loss $\langle C\rangle$ as a function of $\beta\gamma$. Previous measurements, referenced in the text, by NA49, and ALEPH are also shown. The normalization was done to have $\langle C\rangle = 1.0$ for minimum ionizing particles.

It is important to note that the Bethe–Bloch $\mathrm{d}E/\mathrm{d}x$ is different from $\langle C\rangle$. $\mathrm{d}E/\mathrm{d}x$ is the *average* energy loss which is dominated by the tail of the energy loss straggling function, where as $\langle C\rangle$ is related to the peak, Δ_p.

From the resolution obtained for $3\,\mathrm{GeV}/c$ protons (close to MIPs) it is possible to estimate the resolution for the ALICE TPC. In Ref. [1] it was shown that for the given pad segmentation the resolution depends only on the track length. Since the track length in the ALICE TPC is 3.3 times longer (IROC + OROC) than in the prototype, the estimated PID resolution therein is $\sigma_C \sim 9.3\%/\sqrt{3.3} = 5.1\%$.

4.2.1. Comparison with the energy loss model of Bichsel

In this section the results from the beam test, as shown in Fig. 9, are interpreted along a model developed by Bichsel [10]. In his model the energy loss in gases is derived from the Allison Cobb Photo Absorption Ionization process [11], using photo absorption cross-sections from Berkowitz [12].

In the model it is shown that two energy loss straggling functions (or truncated mean distributions) calculated for the same gas, but for different $\beta\gamma$ or segment length, can be related by a two-parameter linear scaling of the abscissa ($x' = \alpha_0 x + \alpha_1$) in the probability distributions. The scaling parameters are evaluated by requiring the two distributions having the same FWHM and integrals. Fig. 10 shows an overlap of the straggling function for $1\,\mathrm{GeV}/c$ protons and the *scaled* straggling function for $3\,\mathrm{GeV}/c$ protons (left), and similarly the overlap of the two truncated mean distributions (right). The close agreement demonstrates the applicability of two-parameter scaling, thus making the tabulation of the distributions easier as only one straggling function is required, the rest being described by their scaling parameters.

This method also suggests a simple way to construct a general fit function.

Bichsel has provided us with straggling functions calculated for 7.5 mm ionization length in pure Neon at the experimental gas density of $\rho = 0.00091\,\mathrm{g/cm^3}$. Fig. 11 shows a direct comparison between his model and our experimental data for $3\,\mathrm{GeV}/c$ protons. The conversion factor (ADC ch/eV) has been adjusted to align the peaks, and the overall normalization is done by requiring the integral to be unity. The agreement between the two

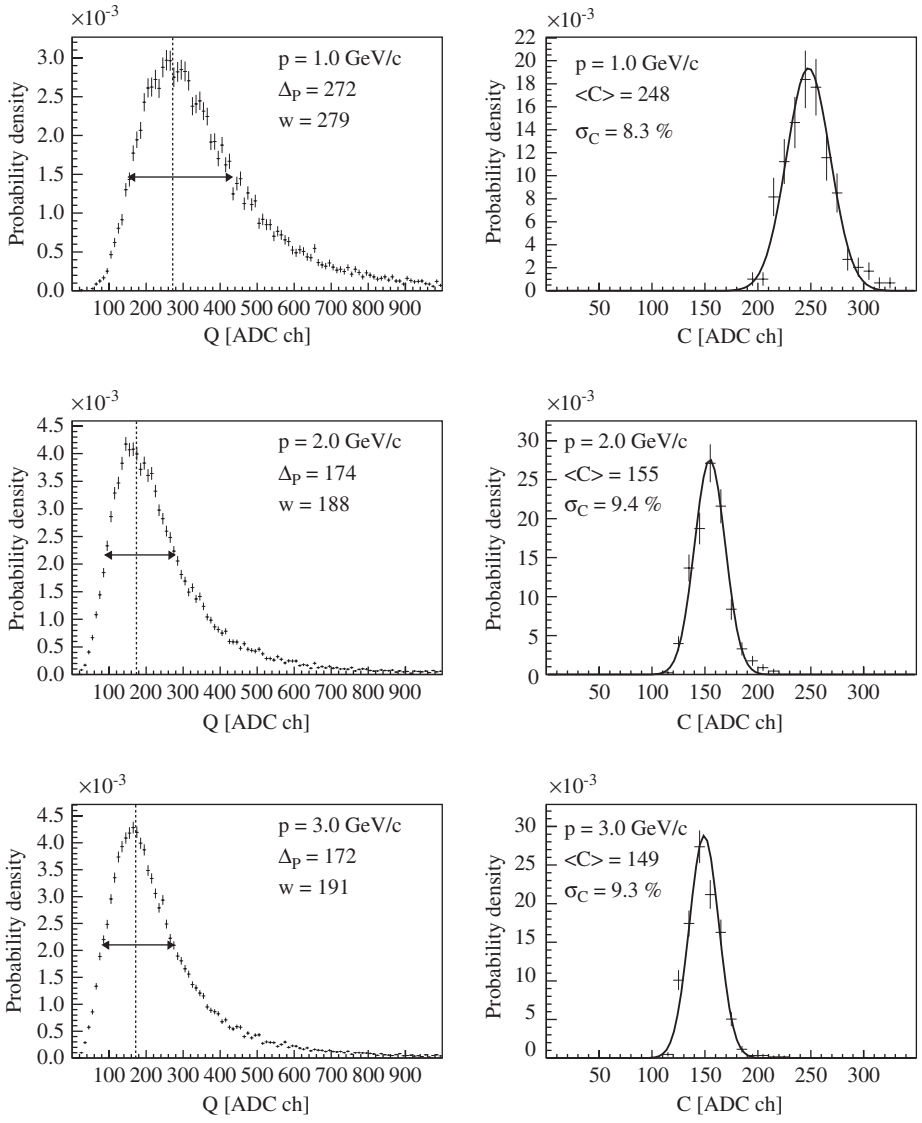

Fig. 9. The straggling functions (left) and the truncated mean distribution (right) for protons with momentum 1–3 GeV/c. Left: The dashed line indicates the most probable value, Δ_p, of the straggling functions while the double arrows shows the FWHM, w. Right: The solid line is a normalized Gaussian fit to the distribution.

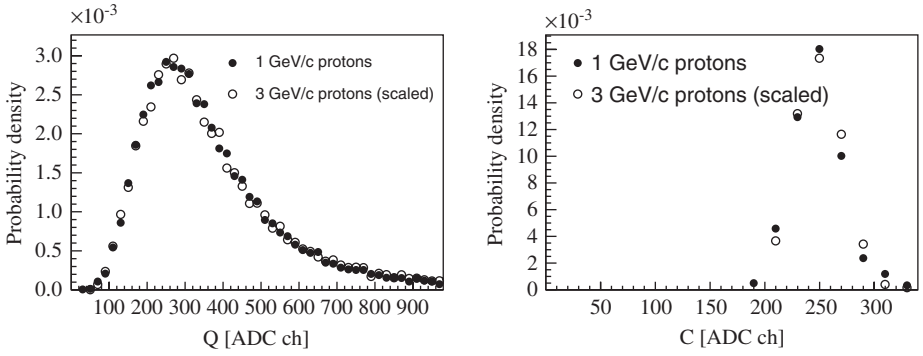

Fig. 10. The 3 GeV/c proton straggling functions (left) and truncated mean distribution (right) scaled to match the 1 GeV/c distribution. The scaling parameters are $\alpha_0 = 1.46$, and $\alpha_1 = 33$, see text.

straggling functions is reasonable, but the extracted resolution from the truncated mean is $\sigma_C = 8.0\%$ in the model and 9.3% for the data (Fig. 9), leaving a discrepancy of 15%.

This discrepancy can be understood from the experimental straggling function. If cluster charges are generated according to the experimental straggling function (Fig. 9)

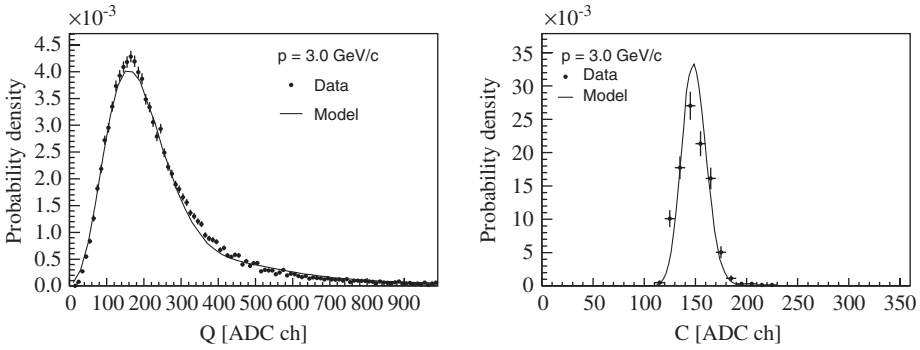

Fig. 11. Comparison of the measured straggling functions and truncated mean distributions (data) to the model of Bichsel (model).

and a virtual track is constructed with the same number of clusters as for the data (60 clusters), the resolution is close to the 8% in agreement with the model. The resolution of the real tracks is deteriorated because the cluster charges are correlated; when cluster charges in neighboring pad rows are compared they exhibit a +33% correlation factor, which reduces the generic information on the track.

The correlations in the data originate from detector effects. The model describes the energy loss in the gas while the experimentally measured quantity is the charge collected on the pads. To adapt the model to this fact a simple simulation was performed. For each single row an energy loss is randomly generated according to the Bichsel model. This energy loss is then converted to the number of electrons given the required energy per electron–ion pair of $W = 30\,\mathrm{eV}$. Each electron is then randomly distributed along the track segment[2] 90 cm away from the pad row and consequently transported, with diffusion taken into account, to the pad plane. Because of the transverse expansion of the electron cloud being on its way to the cathode plane an electron might be collected in another pad row than the one directly opposite to the electron when it was created before drifting. The electron is then amplified according to an exponential distribution and a gain (ADC ch/electron) is fixed to align data and simulation. The gain G was adjusted for each setting; $G(p = 2\,\mathrm{GeV}/c) = G(p = 1\,\mathrm{GeV}/c)/1.055$ and $G(p = 3\,\mathrm{GeV}/c) = G(p = 1\,\mathrm{GeV}/c)/1.026$.[3] In this intuitive simulation the capacitive coupling between adjacent pad rows was not taken into account.

Fig. 12 shows the comparison between the data and the adjusted Bichsel model after the detector effects have been included. From the agreement we conclude that the energy loss mechanism is well described by the model, and that the detector effects are plausibly included in the model.

[2]Since we have no information in the straggling function about the energy loss in individual collisions we distributed the electrons randomly.

[3]This small discrepancy can either be due to a problem with the model or experimental conditions such as gas density variations between runs and/or the absolute calibration of the beam momentum.

This method also fixes the adjustment of the gain to $G(p = 1\,\mathrm{GeV}/c) = 9.6$ ADC ch/electron or an effective amplification gain of 9600.

If the simulated distributions are treated as fits to the truncated mean distributions, the probability of the model describing the data is 21%, 5.7%, and 0.11%, for the $p = 1, 2, 3\,\mathrm{GeV}/c$ data sets, respectively. In all cases, the description of the data is better than the previous Gaussian fit functions in Fig. 9 where there are two fit parameters to optimize. However, the biggest difference between the two approaches is that the model comparison is an independent method of calibrating a TPC (or any other detector based on energy loss) for particle identification based only on the fundamental understanding of the interaction of charged particles with matter rather than on a phenomenological description of the specific experimental data. The parameters necessary for comparing the model with the data should include instrumental effects like e.g. diffusion, gain, capacitive coupling between adjacent pads. The model could also be applied for describing the space point resolution of the detector.

Finally, one can extend the simulation to the full ALICE TPC (IROC + OROC) setup with a maximal drift length of 250 cm, where one estimates an energy loss resolution $\sigma_C = 4.9\%$ for a MIP which is consistent with our earlier estimate based on the track length scaling. On the other hand, in the high occupancy environment of central heavy ion collisions it will be difficult to uniquely associate all clusters with the corresponding tracks, and a resolution deterioration of 1.4% is estimated from simulations [5]. The resolution is still better than that of $\sigma_C/\langle C\rangle \leqslant 7\%$ as stated in the beginning.

5. Summary

The performance of the final ALICE TPC has been studied using the prototype test setup. The main results are:

- The IROC channel noise is well below the required 1000 electrons.

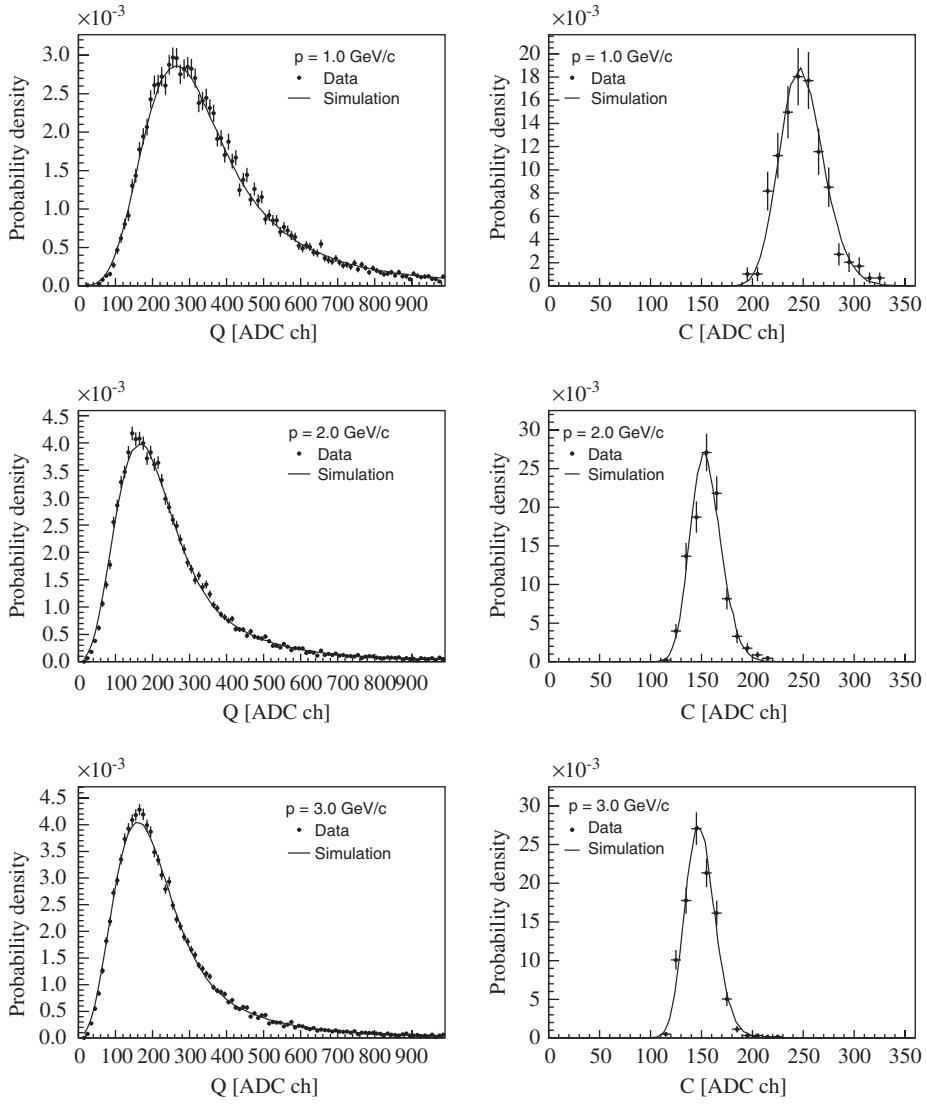

Fig. 12. Comparison of the measured straggling functions and truncated mean distributions (experimental data) to the model of Bichsel with detector effects included (simulation).

- The ALTRO algorithm was successfully applied to correct the pad signals for ion tail distortions.
- The measured space point resolutions in pad ($r\phi$) and time (z) direction fulfills the tracking requirements.
- The measured energy loss resolution agrees with ionization energy loss calculations and facilitates statistical particle identification on the relativistic rise.

All results agree with the ALICE Monte Carlo simulations of the TPC which have been used to study the physics performance of the full system [13].

Acknowledgments

The authors would like to thank the ALICE DAQ and DCS groups for helping prepare the test setups, and Hans Bichsel for many valuable discussions on energy loss in gases, particle identification, and for supplying us with model calculations.

References

[1] ALICE Collaboration, Time Projection Chamber, ALICE TDR 7, CERN/LHCC 2000-001.
[2] C. Garabatos, [ALICE Collaboration], Nucl. Instr. and Meth. A 535 (2004) 197.
[3] ALICE Collaboration, Trigger, Data Acquisition, High Level Trigger, Control System, ALICE TDR.
[4] ALICE DAQ Project, DATE V4 User's Guide, ALICE-INT-20002-036.
[5] F. Carminati, [ALICE Collaboration], et al., J. Phys. G 30 (2004) 1517.
[6] B. Mota, J. Baechler, R. Bramm, R. Campagnolo, R.E. Bosch, A. Jimenez de Parga, L. Musa, Nucl. Instr. and Meth. A 535 (2004) 500.
[7] R. Bramm, Ph.D. Thesis, Johann Wolfgang von Goethe, Universität in Frankfurt am Main, 2005 (arXiv:physics/0501052).

[8] W. Blum, L. Rolandi, Particle Detection with Drift Chambers, Springer, Berlin, ISBN 3-540-56425-X.
[9] B. Lasiuk [NA49 Collaboration], NA49 Note Number 120.
[10] H. Bichsel, Nucl. Instr. and Meth. A 562 (2006) 154, also see the website ⟨http://faculty.washington.edu/hbichsel⟩.
[11] W.W.M. Allison, J.H. Cobb, Ann. Rev. Nucl. Part. Sci. 30 (1980) 253.
[12] J. Berkowitz, Atomic and Molecular Photoabsorption, Academic Press, New York, ISBN 0-12-091841-2.
[13] ALICE Collaboration, ALICE: Physics Performance Report, vol. II.